IOP Publishing and International Atomic Energy Agency Nuclear Fusion
Nucl. Fusion **47** (2007) 746–753 doi:10.1088/0029-5515/47/8/004

Equilibria and stability in partially relaxed plasma–vacuum systems

M.J. Hole[1,a], **S.R. Hudson**[2] **and R.L. Dewar**[1]

[1] Research School of Physical Sciences and Engineering, Australian National University, ACT 0200, Australia
[2] Princeton Plasma Physics Laboratory, PO Box 451, Princeton, NJ 08543, USA

E-mail: matthew.hole@anu.edu.au

Received 31 January 2007, accepted for publication 11 May 2007
Published 17 July 2007
Online at stacks.iop.org/NF/47/746

Abstract
We develop a multiple interface variational model, comprising multiple Taylor-relaxed plasma regions separated by ideal MHD barriers. The magnetic field in each region is Beltrami, $\nabla \times \boldsymbol{B} = \mu \boldsymbol{B}$, and the pressure constant. Between regions the pressure, field strength, and rotational transform may have step changes at the ideal barrier. A principle motivation is the development of a mathematically rigorous ideal MHD model to describe intrinsically 3D equilibria, with nonzero internal pressure, using robust KAM surfaces as the barriers. This article chiefly addresses whether the stability of two interface configurations with continuous rotational transform, but vanishing interface separation, is different from the stability of a single interface configuration with jump in the rotational transform. To make the problem analytically tractable, we derive the equilibria and stability of a multi-interface plasma in a periodic cylinder, generalizing the cylindrical treatment of Kaiser and Uecker (2004 *Q. J. Mech. Appl. Math.* **57** 1–17). For two interfaces with no jump in rotational transform, we show that one eigenmode has in-phase interface displacements, and an eigenvalue that converges to the single barrier case in the limit of vanishing interface width. The complementary eigenmode is out-of-phase, and highly unstable. Physically, the unstable eigenmode is driven by the parallel current, and caused by the high shear required to match the different rotational transform on each interface. In the limit that the interface separation vanishes, the shear and parallel current density become infinite, and the parallel current between the interfaces nonzero. Surfaces with out-of-phase displacements will then collide, unless the amplitude goes to zero as the interface separation goes to zero. These results suggest the hypothesis that KAM barriers with different irrational rotational transform on either side may be allowable without violating nonlinear stability.

PACS numbers: 52.55.−s, 52.55.Hc, 52.65.Kj

(Some figures in this article are in colour only in the electronic version)

1. Introduction

In 1967, Grad [1] showed that in order for a static 3D equilibrium to exist, the pressure gradient (∇p) must be zero in the neighbourhood of every rational flux surface, and poloidal flux ψ_p surfaces must be relinquished. Since this time, this existence problem in 3D geometry has remained controversial. Our working develops a mathematically rigorous model of 3D ideal MHD configurations, in which the pressure is stepped, and ∇p is zero locally in any finite volume.

The original motivation of the 3D equilibrium problem, as proposed by Grad, was the search for a helical field in cylindrical coordinates. Grad reduced the problem to the magnetic differential equation $\boldsymbol{B} \cdot \nabla \zeta = 1$, with ζ a current potential. Next, Grad [1, appendix A] proved that unless stringent conditions are imposed on $\boldsymbol{B}$, the potential ζ is a non-integrable function due to resonances at rational values of the rotational transform ι (or safety factor $q \equiv 1/\iota$). If ζ is non-integrable, then $\boldsymbol{J}$ and the total current are infinite, and the solution unphysical. A more transparent illustration, which elucidates the requirements on $\boldsymbol{B}$ and ∇p for arbitrary 3D configurations involves adding a helical field perturbation $\delta \boldsymbol{B}$ to a 2D field $\boldsymbol{B}_0$ with perfect flux surfaces [2]. The field must always satisfy $\boldsymbol{J} \times \boldsymbol{B} = \nabla p$, hence $\boldsymbol{B}_0 \cdot \nabla p_0 = (\boldsymbol{B}_0 + \delta \boldsymbol{B}) \cdot \nabla (p_0 + \delta p) = 0$. Here, $\boldsymbol{J}$ is the current density and p_0 and δp the unperturbed and perturbed pressures. To first order, we require

$$\delta \boldsymbol{B} \cdot \nabla p_0 = -\boldsymbol{B}_0 \cdot \nabla \delta p. \tag{1}$$

By employing magnetic coordinates (ψ_t, θ_m, ϕ) for $\boldsymbol{B}_0$, with θ_m and ϕ magnetic poloidal and toroidal angles, and linearizing

[a] Author to whom any correspondence should be addressed.

the perturbations

$$\delta p = \sum_m \sum_n p_{mn} \mathrm{e}^{\mathrm{i}(n\phi - m\theta_m)}, \tag{2}$$

$$\frac{\delta \boldsymbol{B} \cdot \nabla \psi_t}{\boldsymbol{B}_0 \cdot \nabla \phi} = \sum_m \sum_n b_{mn} \mathrm{e}^{\mathrm{i}(n\phi - m\theta_m)}, \tag{3}$$

it can be shown that equation (1) reduces to

$$\mathrm{i}(n - mt(\psi_t)) p_{mn} = p_0'(\psi_t) b_{mn}. \tag{4}$$

Here, n and m are toroidal and poloidal mode numbers, and p_{mn} and b_{mn} perturbed pressure and magnetic field Fourier coefficients. For a given (m, n) perturbation within the range $t_{\min} < n/m < t_{\max}$ there will be a flux surface ψ_t resonant with the perturbation (i.e. $t(\psi_t) = n/m$). In general, a nonzero 3D perturbation can exist only if $p_0'(\psi_t) = 0$. As the rationals are dense in the set of real numbers, the condition $p_0'(\psi_t) = 0$ will hence be dense over the set of real ψ_t [3]. The existence of 3D equilibria can hence only be guaranteed providing $\nabla p_0 = 0$.

Ideal MHD configurations with $\nabla p = 0$ are force-free fields, with $\boldsymbol{B}$ satisfying $\nabla \times \boldsymbol{B} = \mu \boldsymbol{B}$. If μ is constant, $\boldsymbol{B}$ is a linear force-free field, or Beltrami field. Such fields were first introduced in to the astrophysical literature over 50 years ago by Lüst and Schlüter [4] and Chandrasekhar [5], amongst others. The motivation for their work was the vanishing of the Lorentz $\boldsymbol{J} \times \boldsymbol{B}$ force, enabling astrophysical stationary state solutions. Woltjer [6] was the first to derive a Beltrami field by trying to minimize the total energy of a pressureless plasma subject to constant helicity. While successfully describing the nature of stable solutions, Woltjer's working did not address how the plasma evolved to the lower energy state. Nearly 20 years later, Taylor [7, 8] addressed this difficulty by two conjectures initially developed to describe turbulent relaxation in the reverse field pinch: magnetic helicity would be roughly conserved during the relaxation process, even in the presence of resistivity, and no other topological invariant would survive the relaxation phase. Since these formative works, a large body of literature has been devoted to force-free fields and Taylor relaxation. In astrophysical plasmas, important applications include coronal loops and accretion disks. In laboratory plasmas, examples include reverse field pinches and spheromaks. The geophysical monograph 'Magnetic Helicity in Space and Laboratory Plasmas' [9] provides an overview, and lists seminal references.

While Taylor's theory is successful in explaining the reversed field pinch, it needs to be extended in order to explain tokamak and stellarators, which experiments show can have a non-trivial pressure profile. To do this, we suggest a model of *multiple* Taylor-relaxed regions, with $\nabla p = 0$ in each region. Each region is separated by an ideal MHD barrier, where pressure jumps are allowed and so a non-trivial pressure profile can be constructed. In the three dimensional case, the ideal interfaces can be chosen to be the (nonresonant) irrational KAM flux surfaces that survive the onset of field line chaos intrinsic to 3D equilibria [10]. The boundary condition across these interfaces is the continuity of the total pressure $[[p + B^2/2]] = 0$, so any pressure jump must be accompanied by a jump in the field strength. In general, discontinuities in the pressure, field strength, and rotational transform are allowed across the ideal MHD barriers.

There are various questions that must be addressed regarding such a model. For example, should the rotational-transform be allowed to jump across the irrational KAM ideal barrier? Assuming that one can construct a multiple-ideal-interface, piecewise-Taylor relaxed equilibrium, is the equilibrium stable to arbitrary deformation of the interfaces? How much control does one have over the rotational transform profile? To address these questions, without introducing the additional complexity associated with the onset of chaotic field lines, this paper presents such an equilibrium model (see section 2) in cylindrical geometry. The simple geometry allows the equilibrium to be solved analytically, and expressions for the stability to be determined as an eigenvalue problem.

Our working builds principally upon a variational model developed by Spies *et al* [11], which comprised a plasma/vacuum/conducting wall system. In Spies the theory is applied to a plasma slab equilibrium, with boundary conditions designed to simulate a torus. Later analysis by Spies [12] extended the plasma model to include finite pressure. In 2004, Kaiser and Uecker [13] analysed the finite pressure model in cylindrical geometry. More recently, Hole *et al* [14] extended the single interface cylindrical treatment of Kaiser and Uecker to multiple interfaces, and demonstrated the existence of partially relaxed Taylor plasmas with tokamak-like magnetic shear profiles. In this work, we perform a stability analysis on stepped pressure profile plasmas in cylindrical geometry. Our working complements work by Hudson *et al* [15], which developed a numerical algorithm for the calculation of Beltrami fields between two interfaces in 3D plasmas. Hudson *et al* section 3 also treat the equilibrium as an eigenvalue problem, showing that for prescribed inner and outer rotational transform, there is an infinity of eigenvalues for μ. Increasing $|\mu|$ eigenvalues correspond to an increasing number of field reversals ($t = \infty$) between the two interfaces, while the sign of μ determines the sign of the magnetic shear.

This paper is arranged as follows: section 2 presents the variational model for the stepped pressure profile equilibria. Equations for equilibrium and perturbed fields are derived, and expressions for plasma stability determined for local and global displacements. Section 3 solves for the equilibrium field in cylindrical geometry, and generates a mapping between different equilibrium constraint representations. Next, section 4 solves for the perturbed field in a cylindrical plasma, and reduces the stability to an eigenvalue equation. The eigenvalue problem is solved numerically for one and two barrier systems. In particular, the stability of a two barrier configuration with continuous rotational transform profile is compared to the single interface configuration with rotational transform jump. Finally, section 5 contains concluding remarks.

2. Multiple interface plasma–vacuum–model

We generalize the analysis of Kaiser and Uecker [13] to an arbitrary number N of Taylor-relaxed states, each separated by an ideal MHD barrier. The system is enclosed by a vacuum,

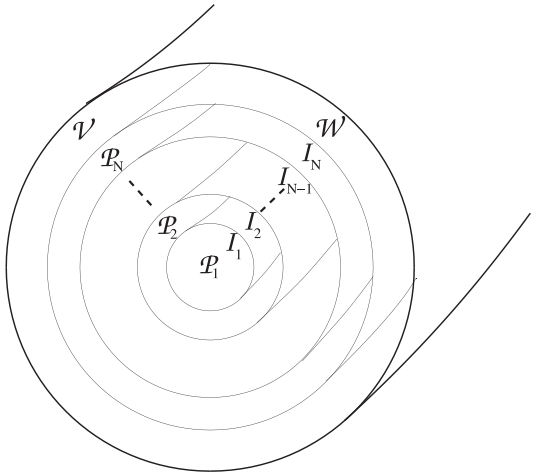

Figure 1. Schematic of magnetic geometry showing ideal MHD barriers $\mathcal{I}_i$, the conducting wall $\mathcal{W}$, plasma regions $\mathcal{P}_i$ and the vacuum $\mathcal{V}$.

and encased in a perfectly conducting wall. For such a system, the energy functional can be written

$$W = \sum_{i=1}^{N} U_i - \sum_{i=1}^{N} \mu_i H_i/2 - \sum_{i=1}^{N} \nu_i M_i, \tag{5}$$

where μ_i and ν_i are Lagrange multipliers, and

$$U_i = \int_{\mathcal{R}_i} \mathrm{d}\tau^3 \left(\frac{P_i}{\gamma - 1} + \frac{B_i^2}{2\mu_0} \right), \tag{6}$$

$$M_i = \int_{\mathcal{R}_i} \mathrm{d}\tau^3 P_i^{1/\gamma}, \tag{7}$$

$$H_i = \int_{\mathcal{R}_i} \mathrm{d}\tau^3 \boldsymbol{A} \cdot \nabla \times \boldsymbol{A} + \oint_{C^{>}_{p,i}} \mathbf{d}\boldsymbol{l} \cdot \boldsymbol{A} \oint_{C^{<}_{t,i}} \mathbf{d}\boldsymbol{l} \cdot \boldsymbol{A} - \oint_{C^{>}_{p,i}} \mathbf{d}\boldsymbol{l} \cdot \boldsymbol{A} \oint_{C^{>}_{t,i}} \mathbf{d}\boldsymbol{l} \cdot \boldsymbol{A}. \tag{8}$$

The term U_i is the potential energy, M_i the plasma mass, and H_i the magnetic helicity in each region $\mathcal{R}_i$. In equations (6)–(8), $\mathrm{d}\tau^3$ is a volume element, γ the ratio of specific heats, and P_i, B_i and $\boldsymbol{A}_i$ the equilibrium pressure, magnetic field strength and vector potential, respectively. The regions $\mathcal{R}_i$ comprise the N plasma regions $\mathcal{R}_1 = \mathcal{P}_1, \ldots, \mathcal{R}_N = \mathcal{P}_N$ and the vacuum region $\mathcal{R}_{N+1} = \mathcal{V}$. Each plasma region $\mathcal{P}_i$ is bounded by the inner and outer ideal MHD interfaces $\mathcal{I}_{i-1}$, and $\mathcal{I}_i$, respectively, whilst the vacuum is encased by the perfectly conducting wall $\mathcal{W}$. Finally, $C^{>}_{p,i}$ and $C^{>}_{t,i}$, and $C^{<}_{p,i}$ and $C^{<}_{t,i}$ are circuits about outer (>) and inner (<) boundaries of $\mathcal{R}_i$ in the poloidal and toroidal directions, respectively. Figure 1 shows the geometry of the system.

Setting the first variation to zero yields the following set of equations:

$$\mathcal{P}_i; \nabla \times \boldsymbol{B} = \mu_i \boldsymbol{B}, \qquad P_i = \text{const}, \tag{9}$$

$$\mathcal{I}_i; \boldsymbol{n} \cdot \boldsymbol{B} = 0, \qquad [[P_i + 1/2B^2]] = 0, \tag{10}$$

$$\mathcal{V}; \nabla \times \boldsymbol{B} = 0, \qquad \nabla \cdot \boldsymbol{B} = 0, \tag{11}$$

$$\mathcal{W}; \boldsymbol{n} \cdot \boldsymbol{B} = 0, \tag{12}$$

where $\boldsymbol{n}$ is a unit vector normal to the plasma interface $\mathcal{I}_i$, and $[[x]] = x_{i+1} - x_i$ denotes the change in quantity x across the interface $\mathcal{I}_i$. The boundary conditions on $\boldsymbol{n} \cdot \boldsymbol{B}$ arise because each interface and the conducting wall is assumed to have infinite conductivity. In turn, these imply the following flux constraints during Taylor relaxation:

$$\mathcal{P}_i; \Psi_i^t = \text{const}, \tag{13}$$

$$\mathcal{V}; \Psi_V^t = \text{const}, \qquad \Psi_V^p = \text{const}, \tag{14}$$

where the subscripts i, V are labels for quantities within the ith plasma region, and vacuum region, respectively, and the superscripts p, t label the poloidal and toroidal fluxes, respectively. Given the vessel with boundary $\mathcal{W}$, the interfaces $\mathcal{I}_i$, and the magnetic field $\boldsymbol{B}$, equations (9)–(12) constitute a boundary problem for the plasma pressure P_i in each region $\mathcal{R}_i$.

The second variation is a straightforward generalization of Spies [11, 12] to multiple interfaces. That is,

$$\delta^2 W = \sum_{i}^{N} \left(\delta^2 W_{P,i} + \delta^2 W_{I,i} \right) + \delta^2 W_V, \tag{15}$$

where

$$\delta^2 W_{P,i} = \int_{\mathcal{P}_i} \mathrm{d}\tau^3 \left(|\nabla \times \boldsymbol{a}|^2 - \mu_i \boldsymbol{a}^* \cdot \nabla \times \boldsymbol{a} + |p_i|^2/\gamma P_i \right), \tag{16}$$

$$\delta^2 W_{I,i} = \int_{\mathcal{I}_i} \mathrm{d}\sigma^2 |\xi_i|^2 [[B\boldsymbol{n} \cdot \nabla B]], \tag{17}$$

$$\delta^2 W_V = \int_{\mathcal{V}} \mathrm{d}\tau^3 |\nabla \times \boldsymbol{a}|^2 \tag{18}$$

and where, following Kaiser and Uecker [13], we have used upper case symbols to denote equilibrium quantities, and lower case represent perturbation. Hence, $\boldsymbol{a}$ is the perturbed vector potential and p_i the perturbation in the equilibrium pressure P_i. Finally, $\xi_i = \boldsymbol{\xi}_i \cdot \boldsymbol{n}$ denotes the normal displacement of I_i.

In Spies [11] the condition $\delta^2 W > 0$ was reformulated as an eigenvalue problem which must be solved iteratively. That is, the functional $\delta^2 W$ was minimized subject to the constraint of constant N_A, where

$$N_A = \int_{\mathcal{P} \cup \mathcal{V}} \mathrm{d}^3\tau |\nabla \times \boldsymbol{a}|^2. \tag{19}$$

To solve the problem the Lagrangian multiplier λ was introduced, and the functional $L = \delta^2 W - \lambda N_A$ varied. Solutions of $\delta L = 0$ with $L = 0$ are stable providing $\lambda > 0$. In the variational formulation of Kaiser and Uecker, $\delta^2 W$ was minimized with respect to $\boldsymbol{a}$ while keeping the displacement ξ of the interface fixed. No normalization appears in this problem, and stability was reduced to the positivity of $\delta^2 W$.

For $N \geqslant 1$, we use a different and more convenient normalization:

$$N_B = \sum_{i}^{N} \int_{\mathcal{I}_i} \mathrm{d}^2\sigma \, |\xi_i|^2, \tag{20}$$

where we have recognized that the displacement of the wall is zero, $\xi_{N+1} = 0$. For $\mathcal{P}_i$, $\mathcal{V}$, $\mathcal{W}$, solutions of $\delta L = 0$ can be

written in terms of the perturbed magnetic field $\boldsymbol{b} = \nabla \times \boldsymbol{a}$ as follows:

$$\mathcal{P}_i;\ \nabla \times \boldsymbol{b} = \mu_i \boldsymbol{b}, \tag{21}$$

$$\mathcal{I}_i;\ \xi_i^*[[\boldsymbol{B}\cdot\boldsymbol{b}]] + \xi_i^*\xi_i[[B(\boldsymbol{n}\cdot\nabla)B]] - \lambda\xi_i^*\xi_i = 0, \tag{22}$$

$$\boldsymbol{n}\cdot\boldsymbol{b}_{i,i+1} = \boldsymbol{B}_{i,i+1}\cdot\nabla\xi_i + \xi_i\boldsymbol{n}\cdot\nabla\times(\boldsymbol{n}\times\boldsymbol{B}_{i,i+1}), \tag{23}$$

$$\mathcal{V};\ \nabla\times\boldsymbol{b} = 0, \tag{24}$$

$$\nabla\cdot\boldsymbol{b} = 0, \tag{25}$$

$$\mathcal{W};\ \boldsymbol{n}\cdot\boldsymbol{b} = 0. \tag{26}$$

Equations (23) and (26) are boundary conditions, and do not result from setting $\delta L = 0$. With a suitable Fourier decomposition chosen, equation (23) solves for the unknown coefficients of the perturbed field in each region. With substitution, equation (22) then becomes a linear eigenvalue equation. The set of equations is completed by expressions for the perturbed fluxes through each region.

3. Cylindrical equilibria

In this section cylindrically symmetric equilibrium solutions are generated. A cylindrical co-ordinate system is used (r, θ, z), with equilibrium variations permitted only in the radial direction. Following Kaiser and Uecker we normalize the plasma–vacuum boundary to $r = 1$, and assume that the cylinder is periodic in the z direction, with periodicity L. In this system, solutions to equations (9)–(12) can be written in vector notation $\boldsymbol{B} = \{B_r(r), B_\theta(r), B_z(r)\}$ as

$$\mathcal{P}_1 : \boldsymbol{B} = \{0, \mathrm{sgn}(\mu_1)k_1 J_1(|\mu_1|r), k_1 J_0(|\mu_1|r)\},$$

$$\mathcal{P}_i : \boldsymbol{B} = \{0, \mathrm{sgn}(\mu_i)\left[k_i J_1(|\mu_i|r) + d_i Y_1(|\mu_i|r)\right], k_i J_0(|\mu_i|r) + d_i Y_0(|\mu_i|r)\},$$

$$\mathcal{V} : \boldsymbol{B} = \{0, B_\theta^V/r, B_z^V\}, \tag{27}$$

where $k_i, d_i \in \mathbb{R}$, and J_0, J_1 and Y_0, Y_1 are Bessel functions of the first kind of order 0, 1, and second kind of order 0, 1, respectively. The terms B_θ^V and B_z^V are constants. The constant d_1 is zero in the plasma core $\mathcal{P}_1$, because the Bessel functions $Y_0(|\mu_1|r)$ and $Y_1(|\mu_1|r)$ have a simple pole at $r = 0$ [16]. The geometry of this system is analogous to the general screw pinch [17], but with key differences. Notably, the pressure gradient is zero, except at ideal MHD barriers, where it is a delta function.

With an analytic form for the equilibrium magnetic field available, the equilibrium problem can now be prescribed in parameter space. Recognizing that the change in pressure can be expressed in terms of the change in field strength B of the barriers, we observe that the plasma equilibrium is completely determined by the magnetic field profile and the radial position of the barriers. That is, the equilibrium is constrained by the $4N + 1$ parameters:

$$\{k_1, \ldots, k_N, d_2, \ldots, d_N, \mu_1, \ldots, \mu_N, r_1, \ldots r_{N-1}, r_w, B_\theta^V, B_z^V\}, \tag{28}$$

where r_i are the radial positions of the N ideal MHD barriers, and r_w the radial position of the conducting wall. Equivalently, the equilibrium can be constrained by the rotational transform and magnetic fluxes. That is, the $4N + 1$ quantities

$$\{\Psi_1^t, \ldots, \Psi_N^t, \Psi_1^p, \ldots, \Psi_{N-1}^p, \Psi_V^t, \Psi_V^p, \iota_1^{\mathrm{in}}, \ldots, \iota_N^{\mathrm{in}}, \iota_1^{\mathrm{out}}, \ldots, \iota_N^{\mathrm{out}}\}, \tag{29}$$

where ι_i^{in} and ι_i^{out} are the rotational transform on the inside and outside of each interface. In cylindrical geometry ι expands as

$$\iota_i^{\mathrm{in}} = \frac{L}{2\pi r_i}\frac{B_{\theta,i}(r_i)}{B_{z,i}(r_i)}, \qquad \iota_i^{\mathrm{out}} = \frac{L}{2\pi r_i}\frac{B_{\theta,i+1}(r_i)}{B_{z,i+1}(r_i)}, \tag{30}$$

whilst the toroidal and poloidal fluxes compute as follows:

$$\Psi_i^t = \int_{r_{i-1}}^{r_i} B_z(r)r\,\mathrm{d}\theta\mathrm{d}r = \frac{2\pi}{\mu_i}\left[k_i r J_1(r\mu_i) + d_i r Y_1(r\mu_i)\right]_{r_{i-1}}^{r_i}, \tag{31}$$

$$\Psi_i^p = \int_{r_{i-1}}^{r_i} B_\theta(r)L\mathrm{d}r = \frac{-L}{\mu_i}\left[k_i J_0(r\mu_i) + d_i Y_0(r\mu_i)\right]_{r_{i-1}}^{r_i}. \tag{32}$$

In the vacuum region, the fluxes compute as

$$\Psi_V^t = B_z^V\pi(r_w^2 - 1), \qquad \Psi_V^p = B_\theta^V L\ln r_w. \tag{33}$$

Figure 2 shows an example with five ideal barriers, with $\mu_1 = 6.0, \mu_2 = 1.2, \mu_3 = 1.1, \mu_4 = 1.0, \mu_5 = 0.9$ and vacuum field $B_\theta^V = 0.0605\,\mathrm{T}$, $B_\theta^V = 0.0676\,\mathrm{T}$. The example is chosen to have tokamak-like ι profile (i.e. increasing safety factor q). In the plasma core, $q = rJ_0(\mu_1 r)/J_1(\mu_1 r)$, which for all $\mu_1 > 0$ is a strictly decreasing function with increasing radius. Elsewhere q may increase or decrease, depending upon the values of d_i/k_i and μ_i. In general, q can jump at the interfaces, although the example shown here is chosen such that $\Delta q = 0$.

4. Stability in cylindrical plasmas

A solution proceeds by Fourier decomposition of the perturbed field $\boldsymbol{b}$ and surface displacements ξ_i of each interface. That is,

$$\boldsymbol{b} = \tilde{\boldsymbol{b}}\mathrm{e}^{\mathrm{i}(m\theta+\kappa z)}, \qquad \xi_i = X_i\mathrm{e}^{\mathrm{i}(m\theta+\kappa z)}, \tag{34}$$

where m, κ are the Fourier poloidal mode-number and axial wavenumber, and $\tilde{\boldsymbol{b}}$ and X_i are complex Fourier amplitudes. Under these substitutions, and after solving for the field in each plasma region, the system of equations (21)–(26) is reduced to the eigenvalue equation,

$$\boldsymbol{\eta}\cdot\boldsymbol{X} = \lambda\boldsymbol{X} \tag{35}$$

with $\boldsymbol{\eta}$ is a $N \times N$ matrix. The ith row of $\boldsymbol{\eta}$ is the ith interface calculation of

$$([[\boldsymbol{B}\cdot\boldsymbol{b}]] + \xi_i[[B(\boldsymbol{n}\cdot\nabla)B]])\,\mathrm{e}^{-\mathrm{i}(m\theta+\kappa z)}, \tag{36}$$

which is the first two terms of equation (22), divided by X_i^*. In equation (36), $\boldsymbol{b}$ and $\boldsymbol{B}$ take values either side of the interface. In regions $\mathcal{R}_i$ and $\mathcal{R}_{i+1}$, equation (23) solves for $\tilde{b}_r$ in terms of equilibrium quantities and the complex amplitudes X_i, X_{i-1} and X_{i+1}, X_i, respectively. As such, $\boldsymbol{\eta}$ is a tridiagonal matrix.

We have solved equation (35) for the set of N eigenvalues $\lambda_1, \ldots, \lambda_N$, and eigenvectors $\boldsymbol{X}_1, \ldots, \boldsymbol{X}_N$ using a standard numerical package. First, using Mathematica, Fortran 90 statements were generated to compute the coefficients of

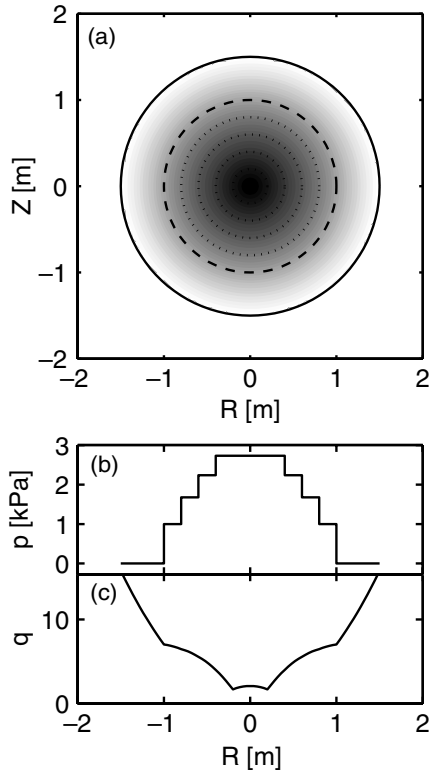

Figure 2. Example stepped pressure plasma profile solution in cylindrical geometry. Panel (*a*) is a shaded contour plot of the polodial flux, where the dashed line is the vacuum boundary and the dotted lines the ideal barriers within the plasma. Panels (*b*) and (*c*) show the pressure profile and safety factor profile, respectively.

the matrix $\boldsymbol{\eta}$ for all cases. For each matrix element η_{ij}, the statements were coded into a case-selection algorithm. To determine the eigenvalue, the QR algorithm for real Hessenberg matrices was employed [18].

When evaluated for an eigenfunction, δL vanishes, and so $\delta^2 W = \lambda N_B$. The system is stable providing there do not exist eigenfunctions with $\lambda < 0$. For each m and magnetic configuration, we have computed the spectrum of eigenvalues as a function of κ. Marginal stability thresholds were investigated by sweeping κ over the range $-K \leqslant \kappa \leqslant K$, with $K = 20$ and $\Delta\kappa = 0.002$, and detecting changes in sign of any of the eigenvalues λ.

For $N = 1$, equation (35) reduces to an expression for the eigenvalue λ. We have benchmarked our variational approach to the results of Kaiser and Uecker [13], in which marginal stability scans are available for a single interface plasma–vacuum cylinder. Figure 3 is a plot of the $m = 1$ marginal stability boundaries in μ_1, δ space, with $r_l = 1.1$, and for a selection of pressure values. Kaiser and Uecker define δ to be a measure of the increase in pitch angle of the field such that

$$B_{\theta,V} = J_1(\mu_1)\cos\delta + J_0(\mu_1)\sin\delta, \tag{37}$$

$$B_{z,V} = J_0(\mu_1)\cos\delta - J_1(\mu_1)\sin\delta. \tag{38}$$

For consistency with our working, we map δ to the jump in ι

$$\Delta\iota = \frac{L}{2\pi}\left(\frac{J_0(\mu_1)/J_1(\mu_1) - \tan\delta}{1 + J_0(\mu_1)/J_1(\mu_1)\tan\delta} - \frac{J_0(\mu_1)}{J_1(\mu_1)}\right)^{-1}. \tag{39}$$

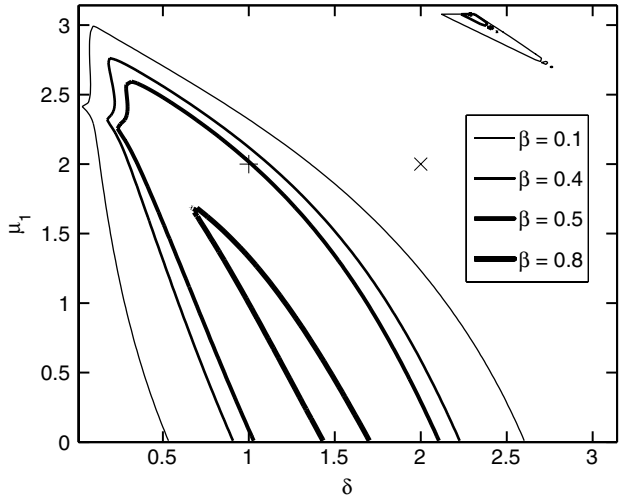

Figure 3. Marginal stability boundaries for $m = 1$ in $\mu_1 - \delta$ space, and for different plasma β values. The parameter μ_1 is the Lagrange multiplier, and δ is a measure of the change in pitch across the plasma–vacuum barrier. The plasma has $r_w = 1.1$ and $L = 1$. The stable region is interior to each locus. The cross-hairs ('x' and '+') denote the equilibrium configuration used for the dispersion curves presented in figures 4 and 6, respectively.

Different internal pressures are described by β. We generalize the definition of Kaiser and Uecker to multiple interfaces,

$$\beta_i = \frac{2\mu_0\langle P_i\rangle}{B^2|_{r=1+}} \tag{40}$$

where $\langle\rangle$ denotes volume averaging. For a single interface, β_1 is related to k_1 through $k_1 = \sqrt{1-\beta}$. Comparison of figure 3 to Kaiser and Uecker [13, figure 3] shows the stability boundaries to be identical. As noted by Kaiser and Uecker, $\delta > 0$ for stability, and so the single plasma–vacuum interface plasmas must have a nonzero jump in rotational transform at the plasma/vacuum boundary for the plasma to be stable. In the limit that $\beta \to 0$, the marginal stability envelope is slightly larger than for $\beta = 0.1$, and so the boundaries are set by current-driven modes.

To develop confidence in the model, we next explore the $m = 1$ stability of two interface ($N = 2$) equilibria, in a configuration in which the position of the internal interface is expected to only weakly perturb the eigenvalue of single interface equilibria. Such a configuration is $\mu_1 = \mu_2 = 2$, $k_1 = k_2 = 0.9486$, $(\beta_1 = \beta_2 = 0.1)$, $d_1 = d_2 = 0$, $\delta = 2$, with separation between the interfaces, $\Delta r = r_2 - r_1$, approaching zero. In the limit that $\Delta r \to 0$ the change in rotational transform is $\Delta\iota = 0.401$. Figure 4 shows a set of $m = 1$ dispersion curves for varying separation Δr. The feature at axial wavenumber $\kappa = -2.57$ corresponds to the outer surface displacement vanishing. The most unstable mode occurs at $\kappa = 0.66$, with $\lambda_1(N = 2) \to \infty$ and $\lambda_2(N = 2) \to 2\lambda(N = 1)$ as the separation between the interfaces approaches zero. For this κ, the stable eigenvalue λ_1 has eigenvector $\boldsymbol{X}_1 = (1/\sqrt{2}, -1/\sqrt{2})$ (surface displacements out-of-phase) and the unstable eigenvalue λ_2 has eigenvector $\boldsymbol{X}_2 = (1/\sqrt{2}, 1/\sqrt{2})$ (surface displacements in-phase). Convergence of λ_2 to the eigenvalue in the single interface configuration benchmarks our analysis in multi-interface configurations.

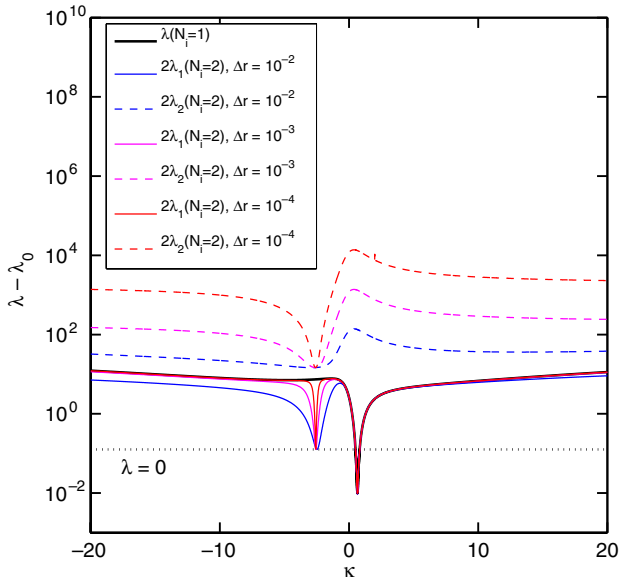

Figure 4. Dispersion curve (eigenvalue $\lambda + \lambda_0$ versus axial wavenumber κ) for $N = 2$ and $m = 1$, and for different separation between interfaces $\Delta r = r_2 - r_1$. Also shown is the dispersion curve ($\lambda + \lambda_0$ versus κ) for $N = 1$ (black). The plasma equilibrium has $\mu_1 = \mu_2 = \delta = 2$ (see cross hairs 'x' in figure 3). The offset $\lambda_0 = \min(\lambda) - 0.01$ is used to permit the dispersion curve to be plotted on a log-log scale. Marginal stability ($\lambda = 0$) is shown by the dotted line.

The analysis of Kaiser and Uecker shows that stable configurations only exist when the edge rotational transform jumps at the plasma–vacuum boundary. To address the question of the stability of these configurations in the continuous rotational transform limit, we add an internal interface and choose the Lagrange multiplier μ_i between interfaces to deliver the required difference in ι. Our aim is to investigate whether barriers with different ι either side of the barrier are allowed without violating stability. We start by defining the equilibrium by the nine parameters

$$\{r_1, r_w, \iota_0, \iota_1^o, \iota_2^{\rm in}, \iota_2^{\rm out}, B^V, \beta_1, \beta_2\} \tag{41}$$

and two constraints $\iota_1^{\rm in} = \iota_1^{\rm out}$ and $\iota_2^{\rm in} = \iota_2^{\rm out}$. The rotational transform at the internal interface (inner and outer sides), and plasma–vacuum interface (inner and outer sides) expand as follows:

$$\iota_0 = \frac{L\mu_1}{4\pi}, \tag{42}$$

$$\iota_1^{\rm in} = \frac{L{\rm sgn}(\mu_1)}{2\pi r_1}\frac{J_1(|\mu_1|r_1)}{J_0(|\mu_1|r_1)}, \tag{43}$$

$$\iota_1^{\rm out} = \frac{L{\rm sgn}(\mu_1)}{2\pi r_1}\frac{J_1(|\mu_2|r_1) + d_2/k_2 Y_1(|\mu_2|r_1)}{J_0(|\mu_2|r_1) + d_2/k_2 Y_0(|\mu_2|r_1)}, \tag{44}$$

$$\iota_2^{\rm in} = \frac{L{\rm sgn}(\mu_2)}{2\pi r_2}\frac{J_1(|\mu_2|r_2) + d_2/k_2 Y_1(|\mu_2|r_2)}{J_0(|\mu_2|r_2) + d_2/k_2 Y_0(|\mu_2|r_2)}, \tag{45}$$

$$\iota_2^{\rm out} = \frac{L}{2\pi r_2}\frac{B_\theta^V}{B_z^V}. \tag{46}$$

Transformation to the representation of equation (28) is afforded via the following five steps:

(i) solve equation (42) for μ_1 and compute $\iota_1^{\rm in}$;

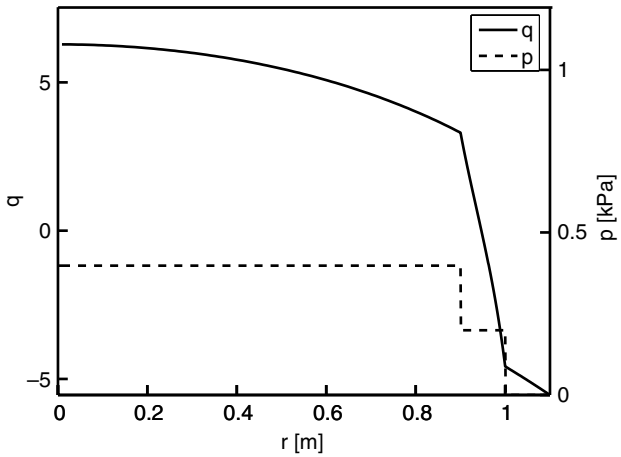

Figure 5. Geometry used for a scan across Δr with no jump in $q = 1/\iota$. The parameters used were $r_w = 1.1$, $\mu_1 = 2.0$, $\delta = 1.0$, $\beta_1 = 0.1$, $\beta_2 = 0.05$, $B^V = 0.1$ T.

(ii) simultaneously solve equations (44), (45) for μ_2 and the ratio d_2/k_2;

(iii) solve equation (46) and $B^{V\,2} = B_\theta^{V\,2} + B_z^{V\,2}$ for B_θ^V, B_z^V;

(iv) using value of d_2/k_2, equation (40) expand $[[p + B^2/(2\mu_0)]] = 0$ on second interface, and solve for k_2;

(v) expand $[[p + B^2/(2\mu_0)]] = 0$ on internal interface, and solve for k_1.

We have chosen $r_2 = 1.0, r_w = 1.1, \mu_1 = 2.0, \delta = 1.0, B^V = 0.1$ T. Both zero and finite beta plasmas have been studied. The internal interface has been placed at $r_1 = r_2 - \Delta r$. Figure 5 illustrates the configuration studied.

Figure 6 is a dispersion curve for the configuration scan for a zero beta plasma, $\beta_1 = \beta_2 = 0$. The two eigenvalues $\lambda_1(N = 2), \lambda_2(N = 2)$ have different qualitative behaviour inside and outside the interval $I_\kappa = \{-2.5 < \kappa < 1.4\}$. Inside I_κ the lower eigenvalue $\lambda_1(N = 2)$ approaches the single interface eigenvalue $\lambda(N = 1)$, but is grossly unstable outside I_κ. Outside I_κ the upper eigenvalue $\lambda_2(N = 2)$ approaches $\lambda(N = 1)$, but inside I_κ, $\lambda_2(N = 2) \gg 1$. In the limit of vanishing interface separation, $\Delta r \to 0$, $\lambda_2(N = 2) \to \infty$. Mode crossings are evident at the I_κ interval bounds $\kappa = -2.5$ and $\kappa = 1.4$.

Linearly, the $\lambda_1(N = 2)$ branch corresponds to current-driven modes made unstable by the high shear required to match different rotational transforms at either interface. As the interface separation decreases, the Lagrange multiplier increases to produce the required high shear. In the limit of zero interface separation, the parallel current density $J_\parallel = \mu_2/\mu_0 B$ in region $\mathcal{P}_2$ becomes infinite, and the parallel current $I_\parallel$ flowing through the region $\mathcal{P}_2$,

$$I_\parallel = \frac{\mu_2 L}{\mu_0}\left(\left(\int r_1{}^{r_2} B_\theta dr\right)^2 + \left(\int r_1{}^{r_2} B_\theta/\iota dr\right)^2\right) \tag{47}$$

is nonzero. It is the presence of this third nonzero singular current (in addition to the singular currents on $\mathcal{I}_1$ and $\mathcal{I}_2$) that modifies the linear stability from equilibria with finite μ_2, and hence zero $I_\parallel$.

Further insight into the behaviour of the two branches is afforded by the surface displacements, shown in figure 7. The

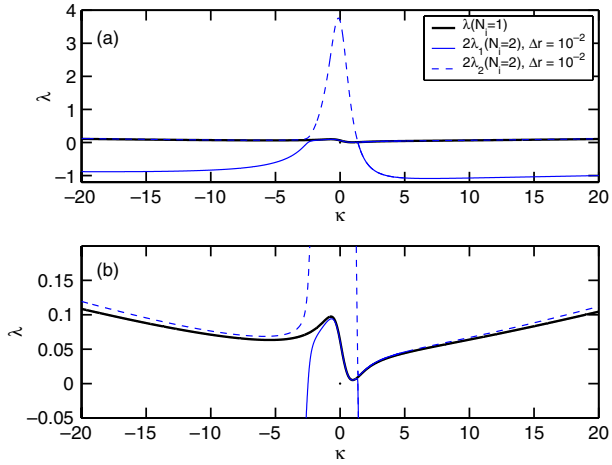

Figure 6. Dispersion curve (2λ versus κ) for $N = 2$ and $m = 1$, for $\Delta r = 0.01$. Also shown is the dispersion curve (λ versus κ) for $N = 1$. The plasma has equilibrium parameters $\mu_1 = \mu_2 = 2$, $\delta = 1$, $\beta_1 = \beta_2 = 0$, with $r_w = 1.1$. Figures (*a*) and (*b*) plot the same dispersion relation on a different vertical scale.

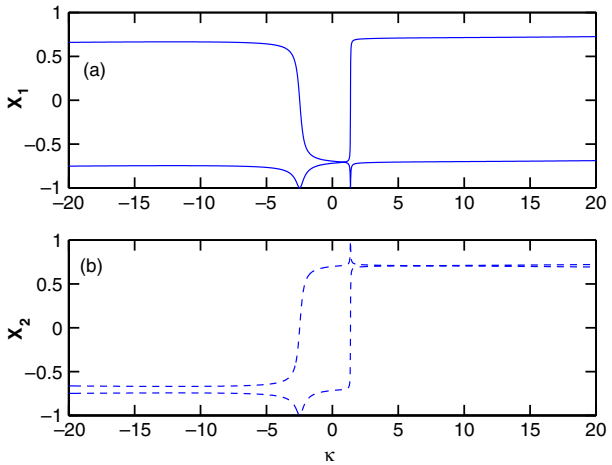

Figure 7. Surface displacements as a function of κ. Figures (*a*) and (*b*) correspond to the solid and dashed dispersion curves in figure 6.

displacements $\boldsymbol{X}_1$ are out-of-phase and in-phase, outside and inside I_κ, respectively. Conversely, the displacements $\boldsymbol{X}_2$ are in-phase and out-of-phase, outside and inside I_κ. In the limit of vanishing interface separation, out-of-phase displacements will collide unless the amplitude also goes to zero.

Figure 7 also reveals mode crossings, corresponding to zeros in one of the displacements in $\boldsymbol{X}_1$ or $\boldsymbol{X}_2$. At $\kappa = -2.5$ for instance, the eigenvalues $\lambda_1(N = 2)$ and $\lambda_2(N = 2)$ have eigenvector $\boldsymbol{X} = (1, 0)$ and $\boldsymbol{X} = (0, 1)$, and so the outer and inner interfaces have zero displacement, respectively.

A convergence test was also performed on the eigenvalues in the limit of vanishing interface separation. Figure 8 plots the eigenvalues at $\kappa = -0.71$ and $\kappa = 0.97$, corresponding to maximum and minimum $\lambda(N = 1)$ in I_κ. As Δr approaches zero, $\lambda_1(N = 2)$ converges to $\lambda(N = 1)$ linearly in Δr. The configuration with the minimum Δr studied in this work was $\Delta r = 10^{-3}$ m, corresponding to $\mu_2 = 1001.6$.

Finally, the dispersion relation is qualitatively unchanged for increasing β. As β increases, the eigenvalue decreases everywhere.

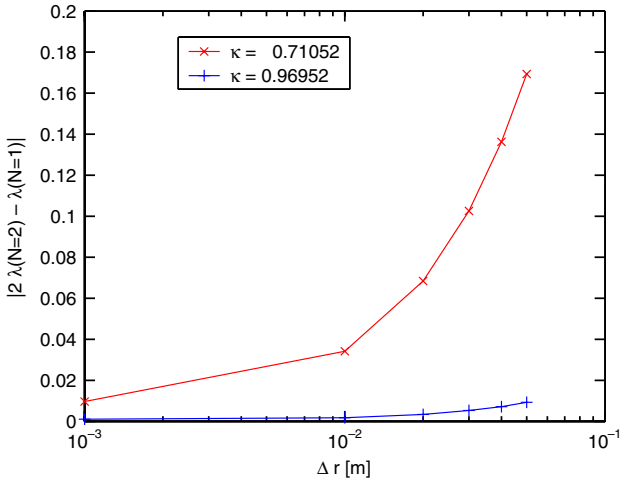

Figure 8. Convergence of eigenvalue as function of vanishing interface separation Δr at two axial wavenumber slices. Plasma equilibrium conditions are the same as in figure 6.

5. Conclusions

We have formulated a variational model for multiple interface stepped pressure profile plasma configurations. The working extends previous treatments, which developed models for a single interface plasma–vacuum system. The motivation for the work is the rigorous development of a model capable of generating 3D ideal MHD equilibria in arbitrary geometry. The system comprises multiple Taylor-relaxed plasma regions, each of which is separated by an ideal MHD barrier of zero width. The system is enclosed by a vacuum region, and encased by a perfectly conducting wall. As a first step, analytic solutions were developed for the equilibrium and perturbed fields of a multiple interface cylinder.

System stability was examined by reducing expressions for the perturbed fields to an eigenvalue problem. For a single interface, marginal stability thresholds reduce to previous working. For plasmas with a second internal interface, across which there is no jump in either rotational transform, μ_i or pressure, system stability converges to the single interface result in the limit of vanishing interface separation. For two interface configurations with continuous rotational transform profile, linear plasma stability is modified from the single interface case with a jump in rotational transform. In the continuous rotational transform profile case, the dispersion curve exhibits eigenvalue mode crossings, corresponding to zeros of the interface displacements. One eigenvalue, corresponding to in-phase surface displacements, approaches the eigenvalue of the single interface configuration with rotational transform jump in the limit of vanishing interface separation. The second eigenvalue, corresponding to out-of-phase surface displacements becomes very unstable. Instability occurs due to the very high shear necessary to match the rotational transform at the interfaces. In the limit of vanishing interface separation the parallel current density between the interfaces becomes infinite, and the parallel current flowing through the region finite. It is the presence of this third nonzero singular current (in addition to the singular currents on the interfaces) that modifies linear stability from that of similar equilibria with nonzero rotational

transform jumps. In the limit of vanishing interface width, linearly unstable out-of-phase displacements collide. We postulate, and will explore in ongoing work, that these out-of-phase displacements are nonlinearly stable. That is, surface displacements vanish with vanishing interface separation.

We have postulated a plasma system with multiple barriers at which the pressure changes and the magnetic shear can reverse or experience a step change. A two barrier plasma, with one barrier internal to the plasma and the other barrier separating plasma and vacuum regions may offer a simple model for internal transport barriers. In future work we will study the stability of such configurations, thereby exploring the energetics of internal transport barrier formation from a variational perspective. We shall also relate the variational approach employed here to an approach generalizing Taylor-relaxed equilibria by augmenting the helicity constraint with other ideal MHD constraints, in the spirit of Bhattacharjee and Dewar [19].

Acknowledgments

The authors would like to acknowledge the support of the Australian Research Council, through grant DP0452728.

References

[1] Grad H. 1967 Toroidal containment of a plasma *Phys. Fluids* **10** 137–54
[2] Boozer A.H. 2004 Physics of magnetically confined plasmas *Rev. Mod. Phys.* **76** 1071–141
[3] Niven I. 1956 *Irrational Numbers* (The Mathematical Association of America) (New York: Wiley)
[4] Lust R. and Schluter A. 1954 *Z. Astrophys.* **34** 263
[5] Chandrasekhar S. 1956 *Proc. Natl. Acad. Sci.* **42**
[6] Woltjer L. 1958 A theorem on force-free magnetic fields *Proc. Natl Acad. Sci.* **44**
[7] Taylor J.B. 1974 *Phys. Rev. Lett.* **33** 1139
[8] Taylor J.B. 1986 Relaxation and magnetic reconnection in plasmas *Rev. Mod. Phys.* **58** 741–63
[9] Brown M.R., Canfield R.C. and Pevtsov A.A. (ed) 1999 *Magnetic Helicity in Space and Laboratory Plasmas* (Washington, DC: American Geophysical Union)
[10] Hudson S.R. 2004 Destruction of invariant surfaces and magnetic coordinates for perturbed magnetic fields *Phys. Plasmas* **11** 677–85
[11] Spies G.O., Lortz D. and Kaiser R. 2001 Relaxed plasma–vacuum systems *Phys. Plasmas* **8** 3652–63
[12] Spies G.O. 2003 Relaxed plasma–vacuum systems with pressure *Phys. Plasmas* **10** 3030–1
[13] Kaiser R. and Uecker H. 2004 Relaxed plasma–vacuum states in cylinders *Q. J. Mech. Appl. Math.* **57** 1–17
[14] Hole M.J., Hudson S.R. and Dewar R.L. 2006 Stepped pressure profile equilibria in cylindrical plasmas via partial taylor relaxation *J. Plasma Phys.* **77** 1167–71
[15] Hudson S.R., Hole M.J. and Dewar R.L. 2007 Rotational-transform boundary value problem for Beltrami fields in toroidal domains *Phys. Plasmas* **14** 052505
[16] Abramowitz M. and Stegun I.A. 1972 *Handbook of Mathematical Functions* (New York: Dover)
[17] Friedberg J.P. 1987 *Ideal Magnetohydrodynamics* (New York: Plenum)
[18] Press W.H., Teukolsky S.A., Vetterling W.T. and Flannery B.P. 1996 *Numerical Receipts in Fortran 77: The art of scientific computing* 2nd edn (Cambridge: University of Cambridge)
[19] Bhattacharjee A. and Dewar R.L. 1982 Energy principle with global invariants *Phys. Fluids* **25** 887